ERDC MP-21-6

US Army Corps
of Engineers®
Engineer Research and
Development Center


# Dimensional Analysis of Structural Response in Complex Biological Structures

Reena R. Patel, David S. Thompson, Guillermo A. Riveros,
Wayne D. Hodo, John F. Peters, Felipe J. Acosta

July 2021



Engineer Research and
Development Center

**The U.S. Army Engineer Research and Development Center (ERDC)** solves the nation's toughest engineering and environmental challenges. ERDC develops innovative solutions in civil and military engineering, geospatial sciences, water resources, and environmental sciences for the Army, the Department of Defense, civilian agencies, and our nation's public good. Find out more at www.erdc.usace.army.mil.

To search for other technical reports published by ERDC, visit the ERDC online library at https://erdclibrary.on.worldcat.org/discovery.

ERDC MP-21-6
July 2021

# Dimensional Analysis of Structural Response in Complex Biological Structures

Reena R. Patel and Guillermo A. Riveros

*Information Technology Laboratory*
*U.S. Army Engineer Research and Development Center*
*3909 Halls Ferry Road*
*Vicksburg, MS 39180*

Wayne D. Hodo

*Geotechnical and Structures Laboratory*
*U.S. Army Engineer Research and Development Center*
*3909 Halls Ferry Road*
*Vicksburg, MS 39180*

David S. Thompson and John F. Peters

*Mississippi State University*
*Starkville, MS 39762*

Felipe J. Acosta

*University of Puerto Rico*
*Mayaguez, PR 00681-9000*

Final report



Prepared for U.S. Army Corps of Engineers
Washington, DC 20314

Under Program Element Number 601102A, Project Number T22, Task 01

# Preface

This study was conducted for the U.S. Army Corps of Engineers, Engineer Research and Development Center under Program Element 60112A, Project Number T22, and Task 01.

The work was performed by the Engineer Research and Development Center, Information Technology Laboratory (ERDC-ITL). At the time of publication, the Deputy Director of ERDC-ITL was Ms. Patti S. Duett, and the Director was Dr. David A. Horner.

This article was originally published online in *International Association for Mathematics and Computers in Simulation* (IMACS) on 9 December 2019.

The support and resources from the ERDC Department of Defense Supercomputing Resource Center are gratefully acknowledged. The authors sincerely thank Dr. Edward Perkins, Dr. Jeffery Hoover, and Dr. Stanley Woodson (all ERDC) for discussions and guidance regarding the topic.

The Commander of ERDC was COL Teresa A. Schlosser and the Director was Dr. David W. Pittman.

# Dimensional Analysis of Structural Response in Complex Biological Structures

**Abstract**

The solution to many engineering problems is obtained through the combination of analytical, computational and experimental methods. In many cases, cost or size constraints limit testing of full-scale articles. Similitude allows observations made in the laboratory to be used to extrapolate the behavior to full-scale system by establishing relationships between the results obtained in a scaled experiment and those anticipated for the full-scale prototype. This paper describes the application of the Buckingham *Pi* theorem to develop a set of non-dimensional parameters that are appropriate for describing the problem of a distributed load applied to the rostrum of the paddlefish. This problem is of interest because previous research has demonstrated that the rostrum is a very efficient structural system. The ultimate goal is to estimate the response of a complex, bio-inspired structure based on the rostrum to blast load. The derived similitude laws are verified through a series of numerical experiments having a maximum error of 3.39%.

## 1. Introduction

The theory of similitude is applicable for testing a scaled, engineering model which is a proxy for the full-scale prototype. A model and prototype are said to have similitude if they have geometric similarity, kinematic similarity and dynamic similarity [9]. Dynamic similarity requires both geometric and kinematic similarity. Hydraulic and aerospace engineering historically are two application areas where similitude has been a mainstay for experimentation using scale models. Any new design concept needs to be scrutinized by rigorous theoretical and experimental verification before it enters the production/manufacturing phase. Tests are generally performed on a model that is similar, in a precise sense, to the prototype. Many times, the parameters involved are so complex that they make prototype testing difficult. In such cases it is beneficial if the tests are done on a model that has

low manufacturing cost and is easy to manage, relative to the prototype. The behavior of the prototype can be predicted from the model by defining a set of relationships that relates relevant characteristics of the prototype to the model [9].

Similarity is defined by a unique set of characteristic parameters that ensure that the non-dimensional governing equations are the same for all similar systems [11,26]. Creating similarity amongst systems assists in forecasting performance of a system based on the results obtained from other similar systems that have already been analyzed or can be studied more easily than the original system. In 1914, E. Buckingham formalized the original method used by Lord Rayleigh and developed the proof of the *Pi* theorem for special cases. The theorem carries his name now [6]. One of the more prominent examples of the power of the application of Buckingham *Pi* analysis is the calculation made by the British Mathematician Taylor in the late 1940s to compute the yield of the first atomic explosion by making estimates based on the photographs of the explosion [24,25].

In the preliminary stages of applying Buckingham *Pi* theorem; the principal quantities controlling the problem are determined along with their dimensional relationships [12]. The Buckingham *Pi* theorem provides a tool to reduce the number of parameters in a problem that need to be investigated. Safoniuk et al. [19] made use of the Buckingham *Pi* theorem to scale a three-phase fluidized bed. This study made use of dynamic and geometric similitude for deriving the scaling laws. Chouchaoui et al. [7] developed scaling laws for the elastic behavior of a laminated cylindrical tube subjected to various loading conditions such as tension, torsion, bending, internal and external pressure, etc. Yazdi and Rezaeepazhand [29] used similitude to design scale models to calculate the flutter pressure of delaminated, composite beam-plates in a supersonic airflow. Ramu et al. [15] established structural similitude for elastic models built from different materials. Their work made use of finite element analysis software for validating the similitude relationships between the model and the prototype. Simitses et al. [16,21–23] carried out several research efforts focused on symmetrically laminated plates to identify the similarity conditions between the model and the prototype. Their research makes use of scaling laws for designing scaled models and uses theoretical methods to compute the model data to predict the behavior of the prototype. Their method restricts the application of similitude principles because an exact or analytical form of the solution must be derived prior to using this methodology for a given set of problems. Ungbhakorn and Singhatanadgid [27] derived the similitude laws for anti-symmetrically laminated plates by applying the similitude transformation directly to the governing differential equations of buckling. In their work, the scaling laws for buckling loads on laminated plates with biaxial loading conditions were derived.

Generally, similitude is used to scale the parameters from a larger-scale prototype to a smaller-scale model. In the current study, similitude is used to scale results obtained from a small-scale computational prototype to a larger-scale model. The computational prototype in the current research is the rostrum of the paddlefish. In preliminary computational experiments, the rostrum has exhibited superior energy dissipation and load bearing capacity when compared to a homogeneous material with a similar geometry [17]. Accordingly, the aim of this study is to develop a set of scaling parameters to scale the computational prototype to a larger size and verify the similitude laws.

This paper is organized as follows: Section 2 gives a general background about the characteristics and function of the rostrum. Section 3 describes the methodology of applying the Buckingham *Pi* theorem for a classical problem with known solution. Section 4 demonstrates the use of Buckingham *Pi* theorem to derive a set of non-dimensional *Pi* terms for a structure subjected to blast load. Section 5 presents the application of the scaling laws developed in Section 4 as well as numerical verification of the derived similarity parameters using finite element analysis.

## 2. Rostrum characteristics and function

The paddlefish (*Polyondon spathula*) can be easily distinguished by the presence of its elongated rostrum as shown in Fig. 1. It is among the most primitive of bony-finned fishes (Osteichthyes, Actinopterygil) and, together with sturgeon, comprises an order of secondary cartilaginous fishes, the Acipenseriformes [14].

### *2.1. Rostrum geometry*

The rostrum of paddlefish is a unique structure comprised of a network of cartilage, tissue, and interlocking star shaped bones called the stellate bones. Fig. 2 shows the stellate bone arrangement in a rostrum of paddlefish. As displayed in Fig. 3, there is interplay between the complex hierarchical lattice architecture and varying material properties in the rostrum. This is typical of biological structures [4,5] and produces uncertainty as to what is dictating

**Fig. 1.** The paddlefish.

**Fig. 2.** Paddlefishrostrum and stellate bone arrangement.

the structural response. Fig. 3(a) shows the cross section of the rostrum highlighting its three components. Fig. 3(b) displays the outer soft tissue layer of the rostrum. Fig. 3(c) shows the inner hard cartilage of the rostrum, which has an elastic modulus an order of magnitude stiffer than the tissue. Fig. 3(d) is representative of the inner soft cartilage of the rostrum whose elastic modulus is an order of magnitude softer than the hard cartilage.

### *2.2. Rostrum function*

The function of the long, paddle-shaped snout is an open question that has received considerable attention. The sensory function of the rostrum enables the fish to detect the type of current [10] allowing them to feed efficiently in both laminar and turbulent currents. Additionally, the sensory function allows the paddlefish to detect tiny zooplanktons without using their visual, chemical, or hydrodynamic senses [28]. The function of the rostrum changes at various stages of the life of paddlefish. In the juvenile stage, the shape of the rostrum is linear and is almost one-third the body length. The primary function of the rostrum at the juvenile stage is sensory. During the sub-adult stage, the shape of the rostrum is spatulate and its primary function is hydrodynamic. During this stage, the paddlefish are active filter feeders. In the adult stage, the shape of the rostrum is linear and the primary function is mechanical.

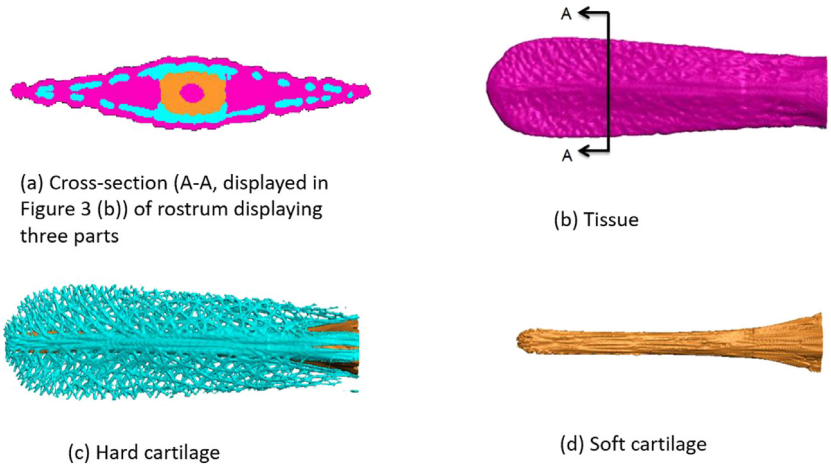


**Fig. 3.** Components of rostrum.

Based on experimental data collected for paddlefish kept in round tanks in the laboratory [20], paddlefish increase their body velocity by about 60 percent during filter feeding. Fish move by contracting muscles that propel their body in the forward direction. During filter feeding, a paddlefish takes in enormous amounts of water in its mouth. The added weight of this water requires more effort during swimming. In addition to this effort, Paddlefish use forward body velocity to transport this water at high velocity. The lift generated by the rostrum during this phase tremendously reduces the amount of effort required by the fish to move at high speed [3,13,17,18].

Fluid–structure interaction (FSI) analysis of the rostrum of the paddlefish revealed interesting hydrodynamic characteristics of the rostrum [13]. The unique geometrical shape, lightness and strength of the paddlefish rostrum promote swimming enhancements when the fish is swimming both against and with the current. It was observed from the FSI simulations that the fish's velocity increased when the fish was swimming in the direction opposite to the flow. When the fish is swimming against the flow, the shape and position of the rostrum generates vortices which help propel the fish in a forward direction. The vortex generation helps the paddlefish maintain the high speed needed for filter feeding and also provides the much-needed lift that prevents a nosedive into the bottom. When the fish is swimming in the direction of the flow, a small velocity enhancement was observed.

## 3. Application of Buckingham *Pi* theorem to a uniform load on fixed plate

As an example of application of the Buckingham *Pi* theorem, consider a rectangular plate with all edges fixed with a uniformly distributed load w over the entire plate as shown in Fig. 4. This case is chosen for analytical validation of similitude because of the resemblance of its boundary conditions to the boundary conditions that will be used in the blast analysis. The critical load $P_{cr}$ of the plate depends on the distributed load $w[FL^{-1}]$, the Young's modulus $E[FL^{-2}]$ of the plate material, the cross sectional moment of inertia $I[L^4]$ of the plate, the vertical deflection $u[L]$ and the length of the plate $l[L]$. $P_{cr}$ can be written for this case as follows:

$$P_{cr} = g(w, E, I, u, l) \tag{1}$$

Application of the Buckingham *Pi* theorem to a general problem can be described as follows. Consider a dimensional quantity $F$ that represents a physical phenomenon and suppose that the dimensional quantities or factors influencing this phenomenon are $\delta_1, \delta_2, \delta_3, \ldots \delta_n$. The relationship between $F$ and the dimensional parameters $\delta_1, \delta_2, \delta_3, \ldots \delta_n$ is given by the following equation:

$$F = g(\delta_1, \delta_2, \delta_3, \ldots \delta_n) \tag{2}$$

In Eq. (2), $F$ is the dependent variable and $\delta_n (n = 1, 2, 3, \ldots, n)$ are the independent variables. Eq. (2) can be non-dimensionalized and expressed as shown in Eq. (3):

$$\pi_1 = f(\pi_2, \pi_3, \pi_4, \ldots \pi_{n-k}) \tag{3}$$

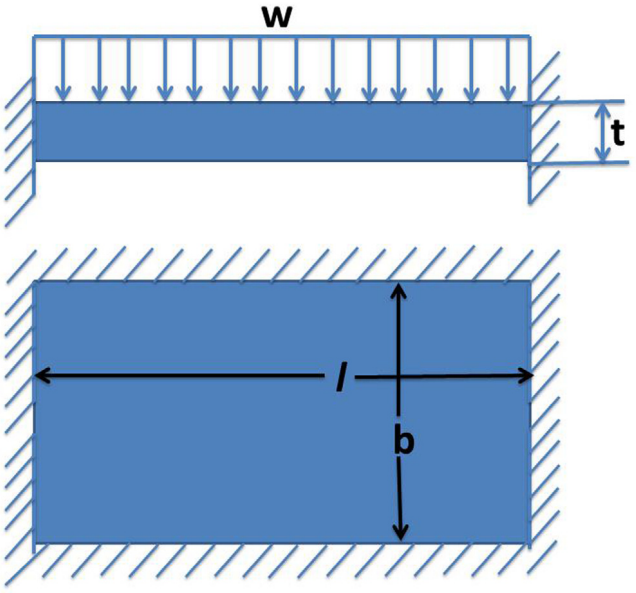


**Fig. 4.** Uniformly loaded plate with all edges fixed.

where $\pi_2, \pi_3, \pi_4, \ldots \pi_{n-k}$ are the dimensionless products of $n$ physical parameters and $k$ is the number of fundamental dimensions (Force, Length, Time) or (Mass, Length, Time) involved in the physical phenomenon.

The similitude requirement stipulates that the $\pi$ terms $\pi_2, \pi_3, \pi_4, \ldots \pi_{n-k}$ must be equal for the model and the prototype if the functional relationship, (i.e., $(\pi_1)_m = (\pi_1)_p$ ), is to be satisfied.

In this example, the number of physical variables, $n$, equals 6 and the number of dimensions, $k$, equals 2. Therefore, there are $n - k = 4$ *Pi* groups. The quantities $P_{cr}[FL^{-2}]$, $w[FL^{-1}]$, $E[FL^{-2}]$, $I[L^4]$, $b[L]$, $t[T]$, and $u[L]$ need to be represented in terms of non-dimensional *Pi* products similar to Eq. (3). The repeating variables are selected in such a way that all the relevant dimensions are represented. For this example *(E, l)* are selected as repeating variables that will be used to nondimensionalize the remaining quantities.

$$P_{cr} = g(w, E, I, u, l) \tag{4}$$

$$\pi_1 = P_{cr} E^a l^b$$
$$\pi_1 = F(\tfrac{F}{L^2})^a L^b$$
$$a = 1; b = -2$$

$$\pi_1 = \frac{P_{cr}}{EL^2} \tag{5}$$

$$\pi_2 = W E^a l^b$$
$$\pi_2 = \tfrac{F}{L^2}(\tfrac{F}{L^2})^a L^b$$
$$a = -1; b = 0$$

$$\pi_2 = \frac{W}{E} \tag{6}$$

$$\pi_3 = I E^a l^b$$
$$\pi_3 = L^4(\tfrac{F}{L^2})^a L^b$$
$$a = 0; b = -4$$

$$\pi_3 = \frac{I}{l^4} \tag{7}$$

**Table 1**
Similitude relations.

| Physical parameters | Scale factor |
|---|---|
| Length | $S$ |
| Area | $S^2$ |
| Volume | $S^3$ |
| Linear displacement | $S$ |
| Moment of inertia | $S^4$ |
| Point load | $S_E S^2$ |
| Line load | $S_E S$ |
| Uniformly distributed surface load | $S_E$ |
| Stress | $S_E$ |

$\pi_4 = u E^a l^b$
$\pi_4 = L(\frac{F}{L^2})^a L^b$
$a = 0; b = -1$

$$\pi_4 = \frac{u}{l} \tag{8}$$

The $Pi$ products represented by Eqs. (5) through (8) are dimensionless. Based on this analysis, the prediction equation given by Eq. (3) is:

$$\pi_1 = f(\pi_2, \pi_3, \pi_4) \tag{9}$$

Hence,

$$\frac{P_{cr}}{El^2} = f(\frac{W}{E}, \frac{I}{l^4}, \frac{u}{l}) \tag{10}$$

The quantities affecting the physical phenomenon under study are integrated in Eq. (10) in terms of the dimensionless $Pi$ products. The functional relationship will be satisfied, (i.e., $(\pi_1)_m = (\pi_1)_p$), if the three non-dimensional parameters $\pi_2, \pi_3, \pi_4$ are equal for the model and the prototype.

Eq. (10) is a generalized equation and can be used to represent any system that is described by the same quantities. Consider the dimensionless term $(\pi_3)_m = (\pi_3)_p$

Therefore,
$\frac{I_m}{l_m} = \frac{I_p}{l_p}$
$I_m = I_p(\frac{l_m^4}{l_p^4})$
where, $S = \frac{L_m}{L_p}$
Now, consider the dimensionless term $(\pi_1)_m = (\pi_1)_p$
$\frac{W_m}{E_m} = \frac{W_p}{E_p}$
$W_m = W_p(\frac{E_m}{E_p})$
$W_m = W_p * S_E$
where, $S_E = \frac{E_m}{E_p}$
Using the repeating variables $E$ and $l$ listed above, Table 1 shows how selected variables are non-dimensionalized.

### *3.1. Analytical verification of similitude relations*

Consider a rectangular plate, with all edges fixed as shown in Fig. 4, loaded by a uniformly distributed $w$ over the entire plate. The length of the plate $L$ is 216 inch, Young's Modulus $E$ is $435.11e^{06} psi$, width $b$ is 36 inch, and thickness $t$ is 6 inch subjected to a uniform load $w$ of 10 lbs/in$^2$. Table 2 shows the effect of scaling on parameters such as weight, maximum displacement, and maximum stress. The values of the constants $\alpha$, $\beta_1$ can be obtained from Table 11.4 in Roark's formulas for stress and strain [30]. From Tables 1 and 2, it can be seen that the maximum displacement and maximum stress follow the similitude relation derived using the Buckingham $Pi$ theorem.

**Table 2**
Analytical verification of similitude relation.

| Scale | Weight $\rho Lbt$ | Maximum displacement $U_{max} = \frac{\alpha w b^4}{Et^3}$ | Maximum stress $\sigma_{max} = \frac{-\beta_1 w b^2}{t^2}$ |
|---|---|---|---|
| S = 1 | $\rho * (216 * 36 * 6) = \rho * 46656$ | $\frac{\rho w}{E} * 7776$ | $-\beta_1 w * 36$ |
| S = 2 | $\rho * (432 * 72 * 12) = \rho * 186624$ $= \rho * 46656 * S^3$ | $\frac{\rho w}{E} * 7776 * 2$ $= \frac{\rho w}{E} * 7776 * S$ | $-\beta_1 w * 36$ |
| S = 4 | $\rho * (864 * 144 * 24) = \rho * 2985984$ $= \rho * 46656 * S^3$ | $\frac{\rho w}{E} * 7776 * 4$ $= \frac{\rho w}{E} * 7776 * S$ | $-\beta_1 w * 36$ |

## 4. Application of Buckingham *Pi* theorem to problems with blast loadings

Analysis using scaling laws can aid in determining the behavior of a structure from the response of a similar model that is scaled geometrically by a parameter $\alpha$. Carrying out full-scale experiments can be expensive and often dangerous if the experiments involve explosives. This is certainly the case for the deformation of a wall in response to a blast load. In such cases, experiments are performed on a smaller-scale model and the results are extrapolated based on a set of scaling laws that relate the model to the prototype. The bio-structure of interest in the current study is rostrum of the paddlefish. An earlier feasibility study conducted on the rostrum led to the conclusion that the non-uniform geometry is a toughening mechanism that mitigates failure [3,13,17,18].

### *4.1. Development of Pi parameters*

The following section will illustrate the use of Buckingham *Pi* theorem to derive a set of non-dimensional *Pi* terms for a structure subjected to blast load. Here, $[F, L, T]$ are selected as the fundamental dimensions. The deformation $d[L]$ experienced by a structure impacted by blast loading depends on the linear dimension $L[L]$, stress or pressure $\sigma[FL^{-2}]$, density $\rho[FL^{-4}T^2]$, energy $e[FL]$, velocity $v[LT^{-1}]$, mass $m[FL^{-1}T^2]$, force $F[F]$, and time $t[T]$. There are 9 parameters and 3 fundamental dimensions, thus $(n-k) = 6$ non-dimensional $Pi$ terms. It follows that, Eq. (2) can be written in the following form

$$d = g(L, \sigma, \rho, e, v, m, f, t) \tag{11}$$

Based on the Buckingham *Pi* theorem $(L, \sigma, v)$ are picked as repeating variables that will be used to non-dimensionalize the others.

$$\pi_1 = dL^a\rho^b v^c$$
$$\pi_1 = LL^a(\tfrac{FT^2}{L^{-4}})^a(\tfrac{L}{T^{-1}})^c$$
$$a = -1; b = 0; c = 0$$
$$\pi_1 = \frac{d}{L} \tag{12}$$

$$\pi_2 = \sigma L^a\rho^b v^c$$
$$\pi_2 = (\tfrac{F}{L^2})L^a(\tfrac{FT^2}{L^{-4}})^b(\tfrac{L}{T^{-1}})^c$$
$$a = 0; b = -1; c = -2$$
$$\pi_2 = \frac{\sigma}{\rho v^2} \tag{13}$$

$$\pi_3 = eL^a\rho^b v^c$$
$$\pi_3 = FLL^a(\tfrac{FT^2}{L^{-4}})^b(\tfrac{L}{T^{-1}})^c$$
$$a = -3; b = -1; c = -2$$
$$\pi_3 = \frac{e}{\rho v^2 L^3} \tag{14}$$

**Table 3**
Relationship between the model and prototype for the variables used in the current analysis.

| Parameters | Scale factor | Scale = 1 | Scale = 2 | Scale = 4 |
|---|---|---|---|---|
| Length (L) | $\alpha$ | 1 | 2 | 4 |
| Mass (M) | $\alpha^3$ | 1 | 8 | 64 |
| Stress ($\alpha$) | 1 | 1 | 1 | 1 |
| Time (t) | $\alpha$ | 1 | 2 | 4 |
| Velocity (V) | 1 | 1 | 1 | 1 |
| Displacement (U) | $\alpha$ | 1 | 2 | 4 |
| Strain ($\epsilon$) | 1 | 1 | 1 | 1 |
| Acceleration (A) | $\frac{1}{\alpha}$ | 1 | 0.5 | 0.25 |

$$\pi_4 = mL^a\rho^b v^c$$
$$\pi_4 = FT^2L^{-}1L^a(\tfrac{FT^2}{L^{-4}})^b(\tfrac{L}{T^{-1}})^c$$
$$a = -3; b = -1; c = 0$$
$$\pi_4 = \frac{m}{L^3\rho} \tag{15}$$
$$\pi_5 = fL^a\rho^b v^c$$
$$\pi_5 = FL^a(\tfrac{FT^2}{L^{-4}})^b(\tfrac{L}{T^{-1}})^c$$
$$a = -2; b = -1; c = -2$$
$$\pi_4 = \frac{f}{L^2v^2\rho} \tag{16}$$
$$\pi_6 = tL^a\rho^b v^c$$
$$\pi_6 = TL^a(\tfrac{FT^2}{L^{-4}})^b(\tfrac{L}{T^{-1}})^c$$
$$a = -1; b = 0; c = 1$$
$$\pi_6 = \frac{tv}{L} \tag{17}$$

Recall, the $Pi$ products displayed by Eqs. (12) through (17) are dimensionless. Based on this, the prediction equation given by Eq. (3) will result in the following equation:

$$\pi_1 = f(\pi_2, \pi_3, \pi_4, \pi_5, \pi_6) \tag{18}$$

Hence,

$$\frac{d}{L} = f(\frac{\sigma}{\rho v^2}, \frac{e}{\rho v^2 L^3}, \frac{m}{L^3\rho}, \frac{f}{L^2v^2\rho}, \frac{tv}{L}) \tag{19}$$

Assuming that the strain rate is constant, Table 3 shows how to scale selected variables using the repeating variables $(L, \sigma, v)$.

### *4.2. Numerical verification of the derived scaling laws*

The developed scaling laws are applied to a complex biological model. In the current research, the commercial software package Abaqus™ [2] is used to perform computational mechanics experiments on the biological model of interest. The description of the model and analysis details follows in the subsequent sections.

#### *4.2.1. Model description*

Numerical experiments are carried out on the paddlefish rostrum to study the effect of blast loadings on this complex bio-structure. In the two cases considered, the rostrum is scaled 2 and 4 times its initial size. Similitude theory is applied to scale the weight of the TNT used in the analysis. The parameters involved in the simulation are

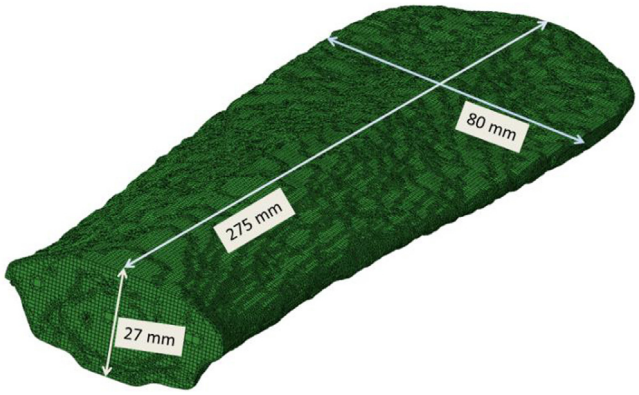


**Fig. 5.** Dimension of the rostrum.

**Table 4**
Rostrum mesh details used in the numerical experiments.

| Rostrum part | Element type [1] | Element shape | Geometric order | Elements |
|---|---|---|---|---|
| Hard cartilage | C3D8 | Hexahedral | Linear | 10 943 |
| | C4D4 | Tetrahedral | Linear | 303 203 |
| | Total nodes | 105 747 | | |
| | Total elements | 314 146 | | |
| Soft cartilage | C3D8 | Hexahedral | Linear | 15 745 |
| | C4D4 | Tetrahedral | Linear | 146 476 |
| | Total nodes | 53 991 | | |
| | Total elements | 162 221 | | |
| Tissue | C3D8 | Hexahedral | Linear | 93 024 |
| | C4D4 | Tetrahedral | Linear | 850 772 |
| | Total nodes | 303 263 | | |
| | Total elements | 943 796 | | |

**Table 5**
Materials used for component parts of rostrum.

| Part | Material |
|---|---|
| Tissue | Vinyl ester epoxy |
| Hard cartilage | Polyethylene fibers |
| Soft cartilage | Polyethylene/Epoxy (as isotropic) |

scaled based on Tables 1 and 3. Fig. 5 shows the numerical model of the rostrum used in the current simulations. The length, width, and the thickness of the model are 275 mm, 80 mm, and 27 mm, respectively. Table 4 gives details of the mesh used in the analysis.

*4.2.2. Material property*

As depicted in Fig. 3 (a through d), the three components of the rostrum exhibit differences in material properties; therefore, these properties are determined from experimental nano-indentation studies carried out on the rostrum [8]. The three materials selected to represent the behavior of the components of the rostrum are shown in Table 5. Tables 6, 7, and 8 depict the material properties of the components of the rostrum model. Polyethylene/Epoxy used for soft cartilage as shown in Table 8 is used as isotropic with the largest value of modulus and strength.

*4.2.3. Force and displacement boundary conditions*

The Abaqus/Explicit$^{TM}$ [2] solver is used for performing the dynamic analysis. Three sets of numerical experiments are carried out on the rostrum. Table 9 shows the details of the trinitrotoluene (TNT) weights and

**Table 6**
Vinyl ester epoxy for the tissue component in rostrum.

| Commercial name | Ashland Derakane® 8084 |
|---|---|
| Elastic modulus | 2.9 GPa |
| Elongation | 8–10% |
| Ultimate tensile strength | 76 MPa |
| Mass density | 1.14 g/cc |

**Table 7**
Polyethylene fibers for hard cartilage component in rostrum.

| Commercial name | Honeywell Spectra® fiber S-900 5600 |
|---|---|
| Elastic modulus | 66 GPa |
| Elongation | 3.5% |
| Ultimate tensile strength | 2.18 GPa |
| Mass density | 1 g/cc |

**Table 8**
Polyethylene/Epoxy (as isotropic) for soft cartilage component in rostrum.

| Commercial name | Polyethylene/Epoxy (as isotropic) |
|---|---|
| E1 | 49,762 MPa |
| E2 | 1,470 MPa |
| G12 | 455 MPa |
| n12 | 0.27 |
| Mass density | 1.05 g/cc |
| F1t | 896.32 MPa |
| F1c | 112.31 MPa |
| F2t | 4.19 MPa |
| F2c | 4.19 MPa |
| F12 | 7.53 MPa |

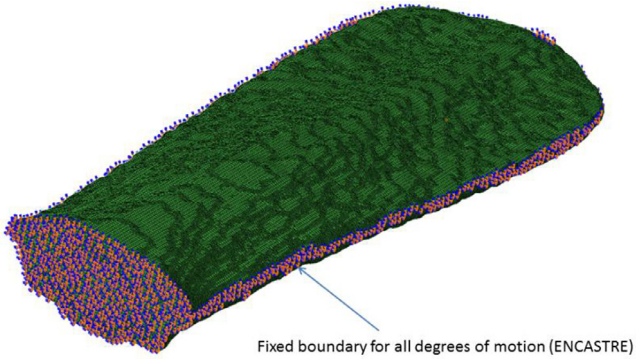


**Fig. 6.** Boundary condition on the rostrum.

time durations of the numerical experiments performed in the current study. Displacement boundary conditions on the edges of the rostrum are fixed for all degrees of motion as depicted in Fig. 6. Fixed boundary conditions are chosen for the edges to hold the rostrum in a stationary position when it is under the influence of the shock wave from the blast load.

**Table 9**
Numerical experiment details.

| Scale | Length of rostrum (mm) | Weight of TNT (kg) | Time duration (s) | Distance between model and TNT (mm) |
|---|---|---|---|---|
| 1 | 275 | 0.02 | 0.025 | 1000 |
| 2 | 550 | 0.16 | 0.05 | 2000 |
| 4 | 1100 | 1.28 | 0.1 | 4000 |

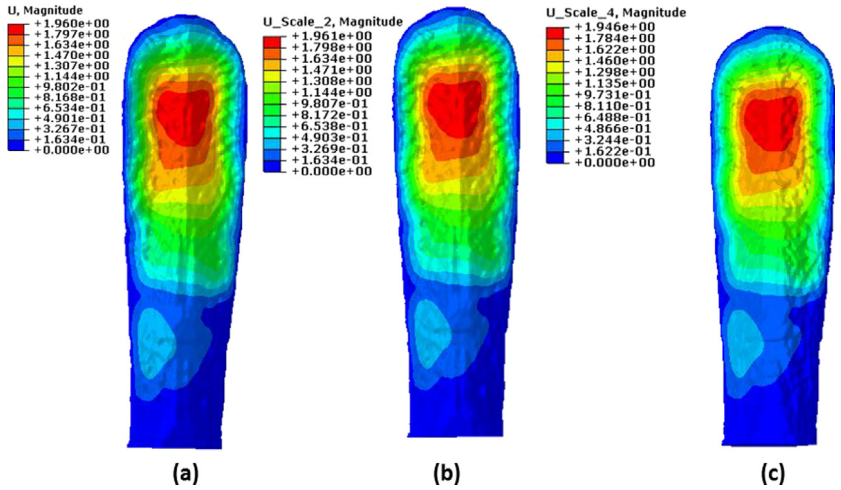


**Fig. 7.** Non-dimensional displacement on top surface of rostrum (a) prototype (b) model scale factor = 2 (c) model scale factor = 4.

## 5. Numerical validation of scaling laws

The scaling laws are validated by comparing the values obtained from the numerical prototype and scaled models with the theoretically expected values from application of Buckingham Pi theorem. The displacement contours for the prototype and model are plotted. Parameters such as displacement and stresses are used for comparison along vertical and horizontal axes of the rostrum. Also, nodal values of displacement, stresses, velocity, and strain are compared for estimating the percentage deviation from the values predicted from the scaling laws.

### *5.1. Displacement contours of the rostrum*

Fig. 7 displays the non-dimensionalized displacement for the model given by Eq. (12) and the prototype. As seen from Fig. 7, the displacement shows qualitatively very similar results for the prototype and scaled model. Since the rostrum has fixed plate boundary conditions applied on all edges, the center of the rostrum experiences maximum displacement. To further analyze the displacement trend, subsequent sections plot the non-dimensional displacement along the horizontal and vertical axes that pass through the region of the rostrum that is experiencing maximum displacement. The minor differences observed in the non-dimensional displacement in Fig. 7 may be attributed to the discretization error of the numerical scheme.

### *5.2. Displacement versus distance along horizontal and vertical axis of rostrum*

Fig. 8 displays the non-dimensional displacement along the vertical axis of the rostrum that is plotted as a function of distance for the prototype and scaled models. Since the rostrum is restrained along its edges, as shown in Fig. 9, zero displacement is observed in these locations. For the models scaled to twice and four times the original model dimensions, the displacement shows nearly identical values along the vertical axis of the rostrum as displayed in Fig. 8. The maximum displacement is observed along the center of the rostrum. This is because the center region is relatively far from the restrained boundary conditions along the rostrum edges. As seen in Fig. 8, two peaks in

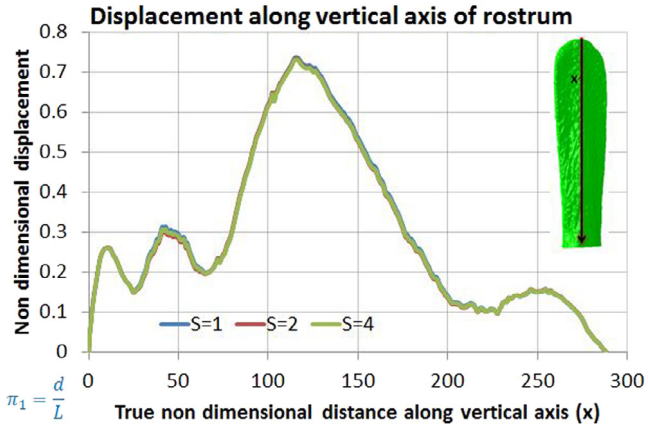


**Fig. 8.** Displacement versus true distance along vertical axis passing through the center of rostrum.

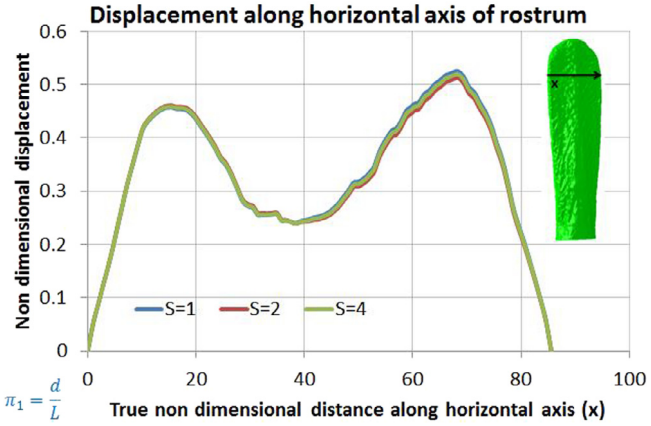


**Fig. 9.** Displacement versus true distance along horizontal axis of rostrum.

displacement are observed at distances of approximately x = 25 mm and x = 50 mm distance from the tip of the rostrum. A third peak is observed at approximately a distance of x = 110 mm from the tip of the rostrum, which also corresponds to the maximum displacement observed along the central vertical axis. This correspondence results from the point charge placement, which is in close proximity to this area of maximal displacement. The displacement steadily decreases along the vertical axis as displayed in Fig. 8. A very small peak is observed around x = 250 mm distance from the tip of the rostrum. The center cartilage is stiffer in this region providing strength and rigidity, thus influencing the displacement.

The non-dimensional displacement shows a similar trend along the vertical axis of the rostrum for the prototype and scaled models as expected from the similitude theory. The scale factors used in the current analysis are S = 2 and S = 4, since the base model is scaled up to 2 and 4 times its original size. The numerical simulation achieved the values as predicted by the Buckingham *Pi* theorem.

Fig. 9 shows the displacement along the horizontal axis of the rostrum located at approximately 63.5 mm from the tip of the rostrum. This position was selected for the horizontal axis because maximum displacement was observed along this axis as depicted in Fig. 7. As before, the non-dimensional displacement is plotted along the horizontal axis for the prototype and the scaled models. Again, very similar quantitative behavior is observed for the prototype and scaled models. As seen in Fig. 9, zero displacement is observed along the edges of the rostrum owing to the restrained boundary condition. A peak is observed in displacement at a distance of 15 mm from the left edge of the rostrum. The displacement decreases near the center bone of the rostrum at a distance of x = 40 mm from the

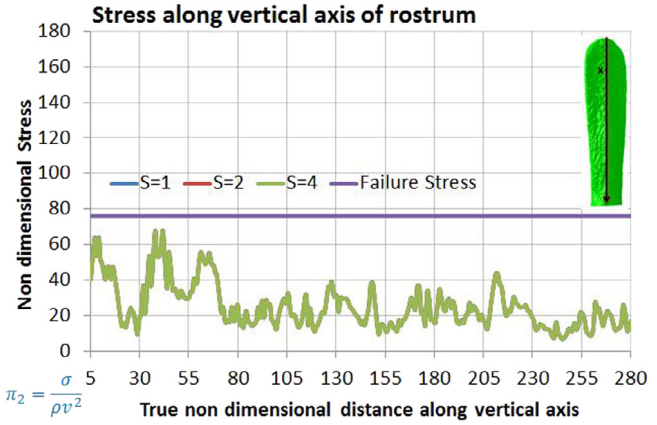


**Fig. 10.** Stress (MPa) versus true distance along vertical axis of rostrum.

left edge. It is observed that the center bone provides stability as observed from the decrease in displacement. At x = 70 mm, another displacement peak is observed. The two displacement peaks are observed near the region of the complex lattice architecture of the rostrum signifying that they are the major load bearing members of the rostrum. This result suggests that, the lattice architecture bears the load while the center bone provides stiffness/stability to the structural system.

### *5.3. Von-Mises stress versus distance along horizontal and vertical axis of rostrum*

Based on the similitude relations used for the current analysis, the stress should be the same for scaled models. Fig. 10 shows the Von-Mises stress along the center bone of the rostrum model.

Identical values of stresses are obtained for the scaled model along the vertical axis of the rostrum when the rostrum is scaled to 2 and 4 times its original size. Also, the stresses observed along the center bone of the rostrum have not crossed the failure stress represented by the purple line in Fig. 10.

Fig. 11 represents the Von-Mises stress along the horizontal axis of the rostrum. The stress pattern and values follow the laws of similitude for the prototype and both scaled cases. The material has reached failure stress in areas where maximum displacement was observed. Owing to the unsymmetrical geometry of the rostrum, the load distribution exhibits an unsymmetrical distribution. The left side of the rostrum shows stresses reaching beyond the failure stress while the right side shows stresses well below the failure stress. Also, the center bone, represented by the $x$-axis distance of 30–60 mm, shows a pronounced reduction in the stresses. Therefore, the center bone is pivotal in providing stability to the system and experiences a significantly low stress level.

### *5.4. Comparison of scaling laws with numerical studies*

Tables 10 and 11 show the comparison of the parameters obtained from the scaling laws and numerical studies conducted on the rostrum. Since the TNT was placed 1000 mm away from the center of the rostrum, the center node shown in Fig. 12 was selected for comparing the scaling laws with numerical results. The physical parameters on the same node are compared for the prototype and the scaled models. As seen in the comparison table the errors are within a maximum of 3.39% percentage. Hence, the numerical experiments have verified the similitude parameters identified by the Buckingham *Pi* theorem within a reasonably acceptable error range. These results, as well as others presented in this section, imply that the selection of parameters used in the Buckingham *Pi* analysis was correct. The small numerical errors may be the result of the discretization error involved in the scheme.

### *5.5. Implementation of scaling laws for cantilever beam boundary condition*

The rostrum in its natural habitat behaves as a cantilever beam with a fixed support near the mouth of the paddlefish. It is subjected to two kind of loads, i.e., its own weight and the hydrodynamic forces. Hence, it possesses

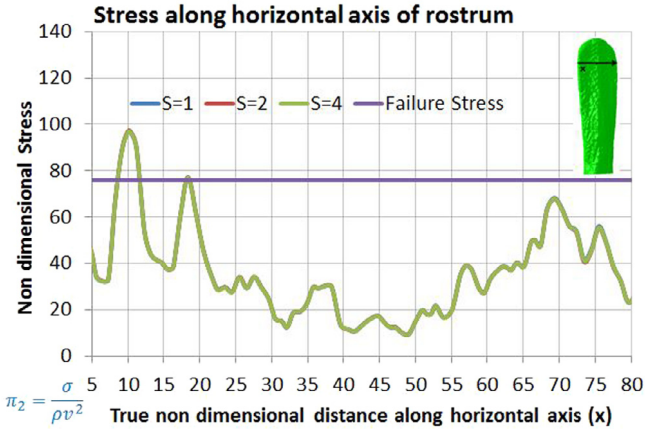


**Fig. 11.** Stress (MPa) versus true distance along horizontal axis of rostrum.

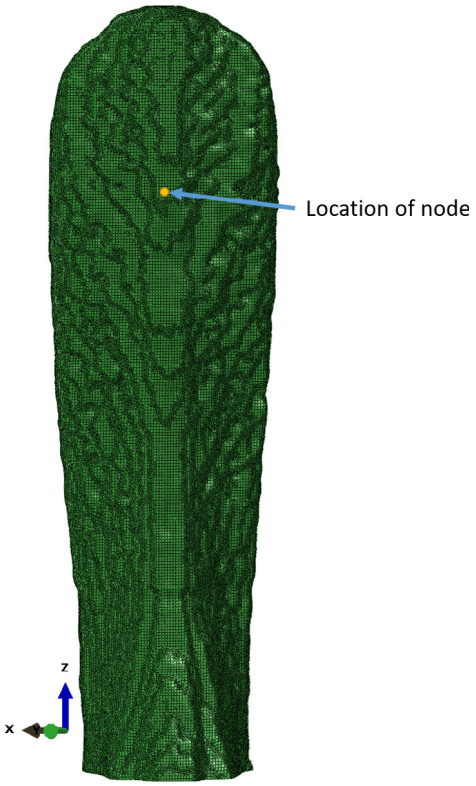


**Fig. 12.** Node selected for comparison of numerical results with scaling laws.

a naturally optimized configuration geared to overcome bending moments. In light of this, the scaling laws developed in the current study are applied to the rostrum with a cantilever beam displacement boundary condition. The force boundary condition is identical to the blast load described in Table 9.

Fig. 13 displays the non-dimensional displacement for the prototype and the scaled model. Since the rostrum is restrained at the bottom with a cantilever beam boundary condition, zero displacement is observed on the base of the rostrum. As seen from Fig. 13, displacement shows an identical trend for the prototype and the scaled models. This again shows that correct parameters were selected for deriving the non-dimensional *Pi* terms.

**Table 10**
Comparison of physical parameters obtained from scaling laws and numerical experiments on the rostrum between prototype and model scaled by a factor of 2.

| Prototype | | Scaled model (S = 2) from scaling laws | From numerical experiment | Percentage error |
|---|---|---|---|---|
| Von Mises stresses in MPa | 21.9543 | 21.9543 | 22.0979 | 0.6541 |
| Maximum principal stresses in MPa | 0.618881 | 0.618881 | 0.601492 | 2.8097 |
| Spatial displacement in mm | 1.92884 | 3.85768 | 3.86485 | 0.1859 |
| Spatial velocity in mm/s | 514.26 | 514.26 | 507.276 | 1.3581 |
| Logarithmic strain in mm/mm | 0.00250712 | 0.00250712 | 0.00251508 | 0.3175 |

**Table 11**
Comparison of physical parameters obtained from scaling laws and numerical experiments on rostrum between prototype and model scaled by a factor of 4.

| Prototype | | Scaled model (S = 4) from scaling laws | From numerical experiment | Percentage error |
|---|---|---|---|---|
| Von Mises stresses in MPa | 21.9543 | 21.9543 | 22.0753 | 0.5511 |
| Maximum principal stresses in MPa | 0.618881 | 0.618881 | 0.597848 | 3.3986 |
| Spatial displacement in mm | 1.92884 | 7.71536 | 7.66811 | 0.6124 |
| Spatial velocity in mm/s | 514.26 | 514.26 | 506.477 | 1.5134 |
| Logarithmic strain in mm/mm | 0.00250712 | 0.00250712 | 0.00251336 | 0.2489 |

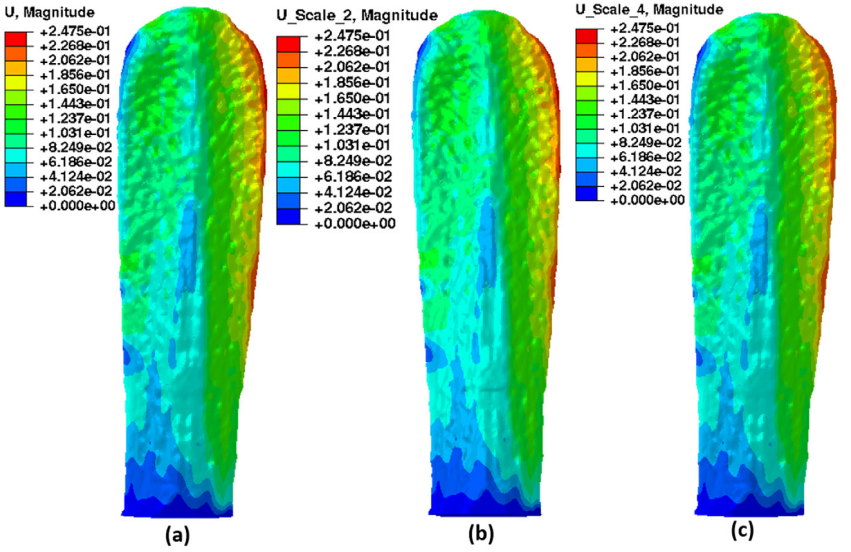


**Fig. 13.** Non-dimensional displacement on top surface of rostrum with cantilever beam displacement boundary condition (a) prototype (b) model scale factor = 2 (c) model scale factor = 4.

## 6. Conclusion

The current research has demonstrated that structural deformation caused by blast impact can be represented in terms of dimensionless $Pi$ terms by application of the Buckingham *Pi* theorem. This study presents the development of similitude relationship for a simple system where the solution is known to verify application of this approach. Numerical experiments were carried out on the rostrum of paddlefish to demonstrate the development and application of similitude laws for blast loading for complex structural models. From the analysis presented, it is evident that deformation, stress, velocity, and strains have been successfully scaled within a reasonably acceptable error range. The strategy presented in this study can be employed to develop and apply similitude relations through the application of the Buckingham *Pi* theorem.

## Acknowledgments

The authors acknowledge the financial support provided by the U.S. Army Engineer Research and Development Center (ERDC) under PE 0601102, Project T22 “Research in Soil and Rock Mechanics”, Task 01. The support and resources from the ERDC DSRC (Engineer Research and Development Center Department of Defense Supercomputing Resource Center) under the subproject Environmental quality modeling and simulation are gratefully acknowledged. The authors sincerely thank Dr. Edward Perkins (ERDC), Dr. Jeffery Hoover (ERDC), and Dr. Stanley Woodson (ERDC) for discussions and guidance regarding the topic. Permission was granted by the Director, Information Technology Laboratory to publish this information.

## References

[1] Abaqus, Abaqus 6.13 Analysis User’s Guide. Online Documentation Help: Dassault Systèmes, 2013.
[2] Abaqus, Providence, RI, USA, ABAQUS Documentation, Dassault Systemes, 2013.
[3] J.B. Allen, G.A. Riveros, Hydrodynamic characterization of the *Polyodon spathula* rostrum using CFD, J. Appl. Math. 2013 (2013).
[4] M.J. Buchler, Tu(r)ning weakness to strength, Nano Today 5 (5) (2010) 379–383.
[5] M.J. Buchler, Y.C. Yung, Deformation and failure of protein materials in physiologically extreme conditions and disease, Nature Mater. 8 (3) (2009) 175–188.
[6] E. Buckingham, On physically similar systems: Illustrations of the use of dimensional equations, Phys. Rev. 4 (1914) 345–376, http://dx.doi.org/10.1103/PhysRev.4.345.
[7] C. Chouchaoui, P. Parks, O. Ochoa, Similitude study for a laminated cylindrical tube under tension, torsion, bending, internal and external pressure, Compos. Struct. 44 (1999) 231–236.
[8] J. Deang, M. Horstemeyer, L. Williams, P. Allison, G. Riveros, Paddlefish rostrum as a structure for bioinspiration: Analysis and modeling of the stress state and strain rate dependence behavior of cartilage, in: TMS Annual Meeting and Exhibition, 2016.
[9] M. Ephraim, O. Thom-Manuel, E. Rowland-Lato, Structural modeling of stability of plane sway frames, Int. J. Civ. Struct. Eng. 2 (2012) 1098–1106.
[10] C. Gurgens, D. Russell, L. Wilkens, Electrosensory avoidance of metal obstacles by the Paddlefish, J. Fish Biol. 57 (2000) 277–290.
[11] S. Kline, Similitude and Approximation Theory, Springer, 2011.
[12] J.D. Logan, Applied Mathematics, fourth ed., Wiley, 2013.
[13] R.R. Patel, G.A. Riveros, Towards Development of Innovative Bio-Inspired Materials by Analyzing the Hydrodynamic Properties of Polodon spathula (Paddlefish) Rostrum, ERDC/ITL 13–4, 2013.
[14] J. Pettigrew, L. Wilkens, Paddlefish and platypus: Parallel evolution of passive electroreception in a rostral bill organ, Sens. Process. Aquatic Environ. (2003) 420–433.
[15] M. Ramu, V.P. Raja, P. Thyla, Establishment of structural similitude for elastic models and validation of scaling laws, KSCE J. Civ. Eng. 17 (2013) 139–144.
[16] J. Rezaeepazhand, G.J. Simitses, J.H. Starnes Jr., Design of scaled down models for stability of laminated plates, AIAA J. 33 (1995) 515–519.
[17] G.A. Riveros, R. Patel, J. Hoover, Swimming and energy dissipation enhancement induced by the rostrum of the paddlefish (*Polyodon spathula*): A multiphysics, fluid-structure interaction analysis, Mater. Res. Soc. Fall Meet. 2015 (2015).
[18] G.A. Riveros, R.R. Patel, J.J. Hoover, Swimmimg enhancement induced by the rostrum of the paddlefish (*Polyodon spathula*) in laminar flows: A multiphysics, fluid-structure interaction analysis, Appl. Math. Model. J. (2020) In review.
[19] M. Safoniuk, J. Grace, L. Hackman, C. Mcknight, Use of dimensional similitude for scale-up of hydrodynamics in three-phase fluidised beds, Chem. Eng. Sci. 54 (1999) 4961–4966.
[20] S.L. Sanderson, J.J. Cech Jr., A.Y. Cheer, Paddlefish buccal flow velocity during ram suspension feeding and ram ventilation, J. Exp. Biol. 186 (1994) 145–156.
[21] G.J. Simitses, J. Rezaeepazhand, Structural similitude for laminated structures, Compos. Struct. 3 (1993) 751–765.
[22] G.J. Simitses, J. Rezaeepazhand, Structural similitude and scaling laws for cross-ply laminated plates, in: Proceedings of the American Society for Composites, Ohio Aerospace Institute Technomic Publishing Co. Inc., 1994, pp. 265–274.
[23] G.J. Simitses, J.H. Starnes Jr., J. Rezaeepazhand, Structural similitude and scaling laws for plates and shells: a review, in: Collection of Technical Papers-AIAA/ASME/ASCE/AHS/ASC Structures, Structural Dynamics and Materials Conference, 2000, pp. 393–403.
[24] S.G. Taylor, The formation of a blast wave by a very intense explosion. I. theoretical discussion, Proc. R. Soc. A 201 (1950) 159–174.
[25] S.G. Taylor, The formation of a blast wave by a very intense explosion. II. theoretical discussion, Proc. R. Soc. A 201 (1950) 175–186.
[26] S. Torkamani, H. Navazi, A. Jafari, M. Bagheri, Structural similitude in free vibration of orthogonally stiffened cylindrical shells, Thin-Walled Struct. 47 (2009) 1316–1330.
[27] V. Ungbhakorn, P. Singhatanadgid, Similitude invariants and scaling laws for buckling experiments on anti-symmetrically laminated plates subjected to biaxial loading, Compos. Struct. 59 (2003) 455–465.
[28] L. Wilkens, D.F. Russell, X. Pei, C. Gurgens, The Paddlefish Rostrum functions as an electrosensory antenna in plankton feeding, Proc. Biol. Sci. 264 (1997) 1723–1729.
[29] A. Yazdi, J. Rezaeepazhand, Structural similitude for flutter of delaminated composite beam-plates, Compos. Struct. 93 (2011) 1918–1922.
[30] W.C. Yound, R.G. Budynas, Roark’s Formulas for Stress and Strain, McGraw-Hill.

# REPORT DOCUMENTATION PAGE

*Form Approved*
*OMB No. 0704-0188*



| 1. REPORT DATE *(DD-MM-YYYY)* | 2. REPORT TYPE | 3. DATES COVERED *(From - To)* |
|---|---|---|
| July 2021 | Final | |

**4. TITLE AND SUBTITLE**

Dimensional Analysis of Structural Response in Complex Biological Structures

**5a. CONTRACT NUMBER**

**5b. GRANT NUMBER**

**5c. PROGRAM ELEMENT NUMBER**
0601102A

**6. AUTHOR(S)**

Reena R. Patel, David S. Thompson, Guillermo A. Riveros, Wayne D. Hodo, John F. Peters, Felipe J. Acosta

**5d. PROJECT NUMBER**
T22

**5e. TASK NUMBER**
01

**5f. WORK UNIT NUMBER**

**7. PERFORMING ORGANIZATION NAME(S) AND ADDRESS(ES)**

See next page.

**8. PERFORMING ORGANIZATION REPORT NUMBER**

ERDC MP-21-6

**9. SPONSORING / MONITORING AGENCY NAME(S) AND ADDRESS(ES)**
U.S. Army Corps of Engineers
Washington, DC 20314

**10. SPONSOR/MONITOR'S ACRONYM(S)**
USACE

**11. SPONSOR/MONITOR'S REPORT NUMBER(S)**

**12. DISTRIBUTION / AVAILABILITY STATEMENT**
Approved for public release; distribution is unlimited.

**13. SUPPLEMENTARY NOTES**
This article was originally published online in *International Association for Mathematics and Computers in Simulation* (IMACS) on 9 December 2019.

**14. ABSTRACT**

The solution to many engineering problems is obtained through the combination of analytical, computational and experimental methods. In many cases, cost or size constraints limit testing of full-scale articles. Similitude allows observations made in the laboratory to be used to extrapolate the behavior to full-scale system by establishing relationships between the results obtained in a scaled experiment and those anticipated for the full-scale prototype. This paper describes the application of the Buckingham *Pi* theorem to develop a set of non-dimensional parameters that are appropriate for describing the problem of a distributed load applied to the rostrum of the paddlefish. This problem is of interest because previous research has demonstrated that the rostrum is a very efficient structural system. The ultimate goal is to estimate the response of a complex, bio-inspired structure based on the rostrum to blast load. The derived similitude laws are verified through a series of numerical experiments having a maximum error of 3.39%.

**15. SUBJECT TERMS**
Rostrum; Bio-structure; Paddlefish; Similitude; Dimensional analysis; Buckingham *Pi* theorem

| 16. SECURITY CLASSIFICATION OF: | | | 17. LIMITATION OF ABSTRACT | 18. NUMBER OF PAGES | 19a. NAME OF RESPONSIBLE PERSON |
|---|---|---|---|---|---|
| a. REPORT | b. ABSTRACT | c. THIS PAGE | | | 19b. TELEPHONE NUMBER *(include area code)* |
| Unclassified | Unclassified | Unclassified | SAR | 21 | |

**7. PERFORMING ORGANIZATION NAME(S) AND ADDRESS(ES)**

Information Technology Laboratory
U.S. Army Engineer Research and Development Center
3909 Halls Ferry Road
Vicksburg, MS 39180

Geotechnical and Structures Laboratory
U.S. Army Engineer Research and Development Center
3909 Halls Ferry Road
Vicksburg, MS 39180

Mississippi State University
Starkville, MS 39762

University of Puerto Rico
Mayaguez, PR 00681-9000